

Magnetotransport properties of the α - T_3 model

Tutul Biswas* and Tarun Kanti Ghosh†

*Department of Physics, Vivekananda Mahavidyalaya, Burdwan-713103, India

†Department of Physics, Indian Institute of Technology-Kanpur, Kanpur-208 016, India

(Dated: September 15, 2016)

Using the well-known Kubo formula, we evaluate magnetotransport quantities like the collisional and Hall conductivities of the α - T_3 model. The collisional conductivity exhibits a series of peaks at strong magnetic field. Each of the conductivity peaks for $\alpha = 0$ (graphene) splits into two in presence of a finite α . This splitting occurs due to a finite phase difference between the contributions coming from the two valleys. The density of states is also calculated to explore the origin of the splitting of conductivity peaks. As α approaches 1, the right split part of a conductivity peak comes closer to the left split part of the next conductivity peak. At $\alpha = 1$, they merge with each other to produce a new series of the conductivity peaks. On the other hand, the Hall conductivity undergoes a smooth transition from $\sigma_{yx} = 2(2n+1)e^2/h$ to $\sigma_{yx} = 4ne^2/h$ with $n = 0, 1, 2, \dots$ as we tune α from 0 to 1. For intermediate α , we obtain the Hall plateaus at values 0, 2, 4, 6, 8, ... in units of e^2/h .

PACS numbers: 72., 71.70.Di, 73.43.-f, 72.80.Vp.

I. INTRODUCTION

The signatures of the Dirac physics in realistic systems have been established after the phenomenal discovery of graphene monolayer^{1,2}. Graphene, a strictly two-dimensional sheet of carbon atoms arranged on a honeycomb lattice (HCL) structure, exhibits low-energy excitations which are linear in momentum. The quasi-particles in graphene obey pseudospin $S = 1/2$ Dirac-Weyl equation. The conduction band meets with the valence band at the six corner points of the hexagonal first Brillouin zone (BZ), known as Dirac points. A number of fascinating physical phenomena have been emerged in graphene in recent years. Unconventional integer quantum Hall effect³⁻⁶ is one of them in which quantization occurs due to the quantum anomaly⁴ of the zero-energy Landau level.

On the other hand, there exists an analogous lattice, the so-called dice or T_3 -lattice^{7,8} in which quasi-particles are characterized by the Dirac-Weyl equation with an enlarged pseudospin $S = 1$. An unit cell of the T_3 -lattice consists of three inequivalent lattice sites. Two of these, usually known as *rim* sites, are situated at the corner points of HCL alternatively. Both the *rim* sites are connected to the three nearest neighbors (NNs). The rest lattice site is called *hub* site. It is located at the center of HCL and is connected to six NNs. The low-energy excitations near the Dirac points consist of three energy branches in which two are linear in momentum, known as conic band. The non-dispersive third energy branch is usually termed as flat band. All the six band-touching points in the first BZ lie on the flat band.

The T_3 -lattice, belongs to bipartite class, has been extensively investigated within the context of topological localization^{7,8}, magnetic frustration^{9,10}, Rashba spin-orbit interaction induced effects¹¹, Klein tunneling¹², plasmon¹³ etc. The existence of T_3 -model has been proposed recently using ultra-cold atoms¹⁴. It is also possible to build a T_3 -lattice by growing trilayer structures of

cubic lattices in the (111) direction¹⁵. Recently, there has been a growing interest on the lattices which are described by the generalized Dirac-Weyl equation with arbitrary pseudospin S ¹⁶⁻¹⁸.

In addition to the T_3 -lattice, there is a modified lattice, known as α - T_3 model¹⁹, in which the hopping strength between the *hub* site and one of the *rim* sites is proportional to the parameter α . A continuous tuning of α demonstrates the crossover between a HCL ($\alpha = 0$) and a T_3 -lattice ($\alpha = 1$). With appropriate doping²⁰ a $\text{Hg}_{1-x}\text{Cd}_x\text{Te}$ quantum well can be mapped onto a α - T_3 model with an effective $\alpha = 1/\sqrt{3}$. The continuous evolution of α is associated with the Berry phase of the system and has an enormous effect on the orbital magnetic response. Particularly, the orbital susceptibility¹⁹ of the system changes from dia- to paramagnetic behavior as one continuously tunes α from $\alpha = 0$ (HCL) to $\alpha = 1$ (T_3). A number of physical observables including DC Hall conductivity²¹, dynamical optical conductivity²¹, and magneto-optical conductivity^{22,23} of a α - T_3 model have been studied recently and the associated behaviors have also been linked with the Berry phase.

In this work, we study the transport properties of the α - T_3 model in a transverse magnetic field within linear response regime. We use Kubo formalism to understand the behavior of the collisional and Hall conductivities with various parameters like electron density and magnetic field. In the strong field regime, the collisional conductivity is described by a number of peaks. For a finite α , the peaks arising in the longitudinal conductivity split because the contributions coming from different valleys are different in a phase. A finite α introduces additional plateaus exactly at the midway between the Hall plateaus obtained in the case of graphene ($\alpha = 0$). We observe a transition in the Hall conductivity from $\sigma_{yx} = 2(2n+1)e^2/h$ (for $\alpha = 0$) to $\sigma_{yx} = 4ne^2/h$ (for $\alpha = 1$) with $n = 0, 1, 2, \dots$.

This paper is presented in the following way. In section II, we discuss basic informations of the system including

Hamiltonian, eigen values, wave functions, and velocity. Various magnetotransport related quantities are derived in section. III. Section IV includes the analysis of the results obtained. We summarize main outcomes of this paper in section V.

II. PRELIMINARY INFORMATIONS OF THE SYSTEM

A. Hamiltonian

Within the framework of the α - T_3 model, there exists three atoms, namely, P, Q, and R in a unit cell as shown in Fig. 1(a). The atoms P and Q form a honeycomb lattice structure analogous to graphene with a hopping amplitude t . The atom R is connected to the atom P via a hopping amplitude αt . The parameter α is the key element of this model. The magnitude of α varies from 0 to 1. The two limiting values of α , namely, $\alpha = 0$ and $\alpha = 1$ represent graphene and dice lattice, respectively.

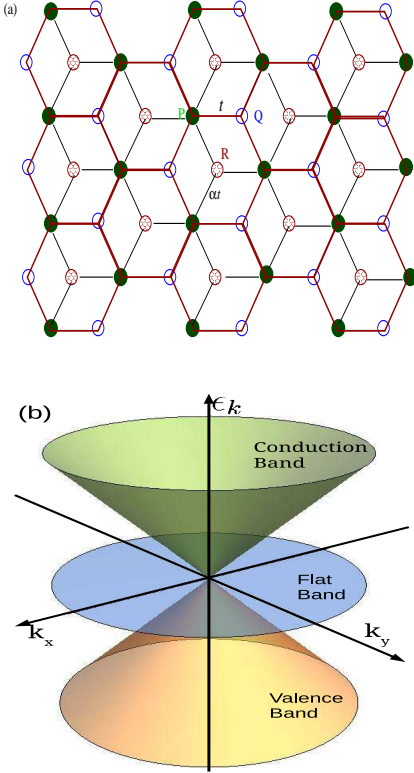


FIG. 1: Sketch of (a) the geometric structure and (b) energy spectrum of a α - T_3 lattice.

Within the tight-binding approximation the low-lying energy states near the Dirac point in a particular valley are described by the Hamiltonian¹⁹

$$H(\mathbf{p}) = \begin{pmatrix} 0 & f_{\mathbf{p}} \cos \phi & 0 \\ f_{\mathbf{p}}^* \cos \phi & 0 & f_{\mathbf{p}} \sin \phi \\ 0 & f_{\mathbf{p}}^* \sin \phi & 0 \end{pmatrix}, \quad (1)$$

where $f_{\mathbf{p}} = v_F(\zeta p_x - i p_y)$ with v_F being the Fermi velocity. The valley index $\zeta = \pm 1$ represents K and K' valley i. e. two inequivalent Dirac points in the first BZ, respectively. The angle ϕ is connected to the parameter α via $\alpha = \tan \phi$.

In presence of an external magnetic field $\mathbf{B} = B\hat{z}$, transverse to the crystal plane, we make the following Pierls substitution $\mathbf{\Pi} = \mathbf{p} + e\mathbf{A}$, where the vector potential \mathbf{A} is chosen in the Landau gauge as $\mathbf{A} = (-By, 0, 0)$. Hence, the Hamiltonian near the Dirac point in the K-valley takes the following form

$$H_K = \gamma_B \begin{pmatrix} 0 & \cos \phi \hat{a} & 0 \\ \cos \phi \hat{a}^\dagger & 0 & \sin \phi \hat{a} \\ 0 & \sin \phi \hat{a}^\dagger & 0 \end{pmatrix}, \quad (2)$$

where $\gamma_B = \sqrt{2}\hbar v_F/l_0$ with $l_0 = \sqrt{\hbar/(eB)}$ being the magnetic length. The annihilation and creation operators are given by $\hat{a} = v_F \Pi_- / \gamma_B$ and $\hat{a}^\dagger = v_F \Pi_+ / \gamma_B$, respectively, with $\Pi_\pm = \Pi_x \pm i\Pi_y$. The operators do obey the commutation relation $[\hat{a}, \hat{a}^\dagger] = 1$ and the actions of them on the Fock states $|n\rangle$ are the following: $\hat{a}|n\rangle = \sqrt{n}|n-1\rangle$ and $\hat{a}^\dagger|n\rangle = \sqrt{n+1}|n+1\rangle$. The Hamiltonian corresponding to the K'-valley is obtained through the substitution $\hat{a} \rightarrow -\hat{a}^\dagger$.

B. Conic band

In the absence of magnetic field the conic band of the α - T_3 model consists of conduction and valence bands which disperse linearly with momentum (see Fig. 1(b)). A perpendicular magnetic field causes to break the continuous energy branches into Landau levels.

On diagonalizing Eq. (2), the energy spectrum of the system can be obtained in the following form

$$\epsilon_{n,\zeta}^\lambda = \lambda \gamma_B \sqrt{n + \chi_\zeta}, \quad (3)$$

where $n = 0, 1, 2, \dots$ and $\lambda = \pm 1$ denotes the conduction band and valence band, respectively. The quantity χ_ζ depends on the valley index ζ through $\chi_\zeta = [1 - \zeta \cos(2\phi)]/2$.

The eigenfunction for $n > 0$ corresponding to the K-valley is given by

$$\Psi_{n,k_x}^{\lambda,K}(\mathbf{r}) = \frac{1}{\sqrt{2}} \begin{pmatrix} \frac{\sqrt{n(1-\chi_+)}}{\sqrt{n+\chi_+}} \Phi_{n-1}(y) \\ \lambda \Phi_n(y) \\ \frac{\sqrt{(n+1)\chi_+}}{\sqrt{n+\chi_+}} \Phi_{n+1}(y) \end{pmatrix} \frac{e^{ik_x x}}{\sqrt{2\pi}}. \quad (4)$$

Here, $\Phi_n(y) = \sqrt{1/(2^n n! \sqrt{\pi} l_0)} e^{-(y-y_0)^2/(2l_0^2)} H_n[(y-y_0)/l_0]$ with $y_0 = l_0^2 k_x$ is the usual harmonic oscillator wave function.

For $n = 0$ the eigenfunction is given by

$$\Psi_{0,k_x}^{\lambda,K}(\mathbf{r}) = \frac{1}{\sqrt{2}} \begin{pmatrix} 0 \\ \lambda \Phi_0(y) \\ \Phi_1(y) \end{pmatrix} \frac{e^{ik_x x}}{\sqrt{2\pi}}. \quad (5)$$

C. Flat band

In addition to the spectrum (Eq. (3)), there exist a non-dispersive energy band $\varepsilon_n^F = 0 \forall n$, known as flat-band.

The corresponding eigenfunctions for the K-valley can be obtained as

$$\Psi_{n,k_x}^{F,K}(\mathbf{r}) = \begin{pmatrix} -\frac{\sqrt{(n+1)\chi_+}}{\sqrt{n+\chi_+}}\Phi_{n-1}(y) \\ 0 \\ \frac{\sqrt{n(1-\chi_+)}}{\sqrt{n+\chi_+}}\Phi_{n+1}(y) \end{pmatrix} \frac{e^{ik_x x}}{\sqrt{2\pi}} \quad (6)$$

and

$$\Psi_{0,k_x}^{F,K}(\mathbf{r}) = \begin{pmatrix} 0 \\ 0 \\ \Phi_0(y) \end{pmatrix} \frac{e^{ik_x x}}{\sqrt{2\pi}}, \quad (7)$$

for $n > 0$ and $n = 0$, respectively.

The eigenfunctions corresponding to the K'-valley are given in the Appendix A.

D. Velocity operators

The components of the velocity for the K-valley can be obtained in the following matrix form

$$v_x = \frac{\partial H}{\partial p_x} = v_F \begin{pmatrix} 0 & \cos \phi & 0 \\ \cos \phi & 0 & \sin \phi \\ 0 & \sin \phi & 0 \end{pmatrix} \quad (8)$$

and

$$v_y = \frac{\partial H}{\partial p_y} = v_F \begin{pmatrix} 0 & -i \cos \phi & 0 \\ i \cos \phi & 0 & -i \sin \phi \\ 0 & i \sin \phi & 0 \end{pmatrix}. \quad (9)$$

To find the velocity components for the K'-valley, we need to make the replacement $v_x \rightarrow -v_x$ and $v_y \rightarrow v_y$.

III. MAGNETO-TRANSPORT COEFFICIENTS

In the regime of linear response theory, where the electric field is weak enough, we will derive here the analytical expressions for the components of the conductivity tensor. To do this we would employ the well-known Kubo formalism²⁴. The diagonal components of the conductivity tensor, known as longitudinal conductivity consists of diffusive and collisional contributions. In presence of perpendicular magnetic field, the diffusive contribution would give vanishing result since the diagonal elements of the velocity matrix are zero. Hence, the contribution in the longitudinal conductivity entirely comes from the collisional or hopping process. The off-diagonal component is usually termed as transverse or the Hall conductivity.

A. Collisional conductivity

Within the Kubo formalism, the general expression for the collisional conductivity is given by²⁵⁻²⁸

$$\sigma_{yy} = \frac{\beta e^2}{S} \sum_{\xi, \xi'} f(\varepsilon_\xi) \{1 - f(\varepsilon_{\xi'})\} W_{\xi\xi'} (y_\xi - y_{\xi'})^2, \quad (10)$$

where $\xi \equiv (n, k_x, \lambda)$ represents the set of all quantum numbers, S is the area of the sample, $\beta = 1/(k_B T)$ with T being the temperature of the system, $y_\xi = \langle \xi | y | \xi \rangle$, and $f(\varepsilon_\xi) = [e^{\beta(\varepsilon_\xi - \mu)} + 1]^{-1}$ is the Fermi-Dirac distribution function with μ as the chemical potential. In addition, $W_{\xi\xi'}$ denotes the probability by which an electron makes a transition from an initial state $|\xi\rangle$ to a final state $|\xi'\rangle$. In the case of elastic scattering by static impurities, its expression is given by

$$W_{\xi, \xi'} = \frac{2\pi n_{\text{im}}}{\hbar S} \sum_{\mathbf{q}} |U(\mathbf{q})|^2 |F_{\xi, \xi'}|^2 \delta(\varepsilon_\xi - \varepsilon_{\xi'}), \quad (11)$$

where n_{im} is the density of impurities and $U(\mathbf{q})$ is the Fourier transform of the screened Coulomb potential $U(\mathbf{r}) = e^2 e^{-k_s r} / (4\pi\epsilon_0\epsilon_r r)$ with ϵ_0 , ϵ , and k_s as the free space permittivity, dielectric constant of the medium, and screened wave vector, respectively. The expression of $U(\mathbf{q})$ is given by $U(\mathbf{q}) = e^2 / (4\pi\epsilon_0\epsilon_r \sqrt{q^2 + k_s^2})$. Finally, $F_{\xi, \xi'}$ denotes the form factor which is defined as $F_{\xi, \xi'} = \langle \xi' | e^{i\mathbf{q}\cdot\mathbf{r}} | \xi \rangle$. The square of $F_{\xi, \xi'}$ for the valley ζ can be obtained as

$$\begin{aligned} |F_{\xi, \xi'}^\zeta|^2 &= \frac{1}{4} \frac{n!}{n'} u^{n-n'} e^{-u} \left[\frac{n'(1-\chi_\zeta)}{\sqrt{(n+\chi_\zeta)(n'+\chi_\zeta)}} L_{n-1}^{n'-n}(u) \right. \\ &\quad + \frac{(n+1)\chi_\zeta}{\sqrt{(n+\chi_\zeta)(n'+\chi_\zeta)}} L_{n+1}^{n'-n}(u) \\ &\quad \left. + \lambda\lambda' L_n^{n'-n}(u) \right]^2 \delta_{k'_x, k_x + q_x}, \end{aligned} \quad (12)$$

where $u = q^2 l_0^2 / 2$.

To derive an analytical expression for the longitudinal conductivity we note that $y_\xi = k_x l_0^2$ and $y_{\xi'} = k'_x l_0^2$. With the virtue of $\delta_{k'_x, k_x + q_x}$ given in Eq. (13), we can write $(y_\xi - y_{\xi'})^2 = q_x^2 l_0^4$. We now restrict ourselves to consider only the intra-band ($\lambda' = \lambda$) and intra-level ($n' = n$) scattering because of the presence of the term $\delta(\varepsilon_\xi - \varepsilon_{\xi'})$ in Eq. (11). With this consideration the form factor for a particular valley ζ simplifies as

$$\begin{aligned} |F_{n, \lambda}^\zeta|^2 &= \frac{1}{4} e^{-u} \left[\frac{n(1-\chi_\zeta)}{n+\chi_\zeta} L_{n-1}(u) + L_n(u) \right. \\ &\quad \left. + \frac{(n+1)\chi_\zeta}{n+\chi_\zeta} L_{n+1}(u) \right]^2 \delta_{k'_x, k_x + q_x}. \end{aligned} \quad (13)$$

For $n = 0$, we have $|F_{0, \lambda}^\zeta|^2 = e^{-u} (1 - u/2)^2$ for both the valleys. Note that both $|F_{n, \lambda}^\zeta|^2$ and $|F_{0, \lambda}^\zeta|^2$ are independent of λ .

The sharp Landau levels broaden due to the presence of the impurities in the system. Assuming Lorentzian broadening, we may write $\delta(\varepsilon_\xi - \varepsilon_{\xi'}) = (1/\pi)\Gamma_0/[(\varepsilon_\xi - \varepsilon_{\xi'})^2 + \Gamma_0^2]$, where Γ_0 is the broadening parameter. It may depend on magnetic field, quality of samples etc. For intra-level and intra-band scattering we may further write $\delta(\varepsilon_\xi - \varepsilon_{\xi'}) \simeq 1/(\pi\Gamma_0)$. Because of the presence of the term e^{-u} in the expressions of $|F_{n,\lambda}^\zeta|^2$, only small values of q^2 are favorable. Hence, $U(\mathbf{q})$ can be approximated as $U(\mathbf{q}) \simeq e^2/(4\pi\epsilon_0\epsilon k_s) \equiv U_0$. We also note that $\sum_{k_x} \rightarrow g_s S/(2\pi l_0^2)$ with g_s being the spin-degeneracy and $\sum_{\mathbf{q}} \rightarrow S/(2\pi)^2 \int q dq d\theta$, where θ is the polar angle of \mathbf{q} .

Combining all these, one may arrive at the following formula

$$\sigma_{yy} = \frac{g_s e^2 \beta n_{\text{im}} U_0^2}{\pi \hbar \Gamma_0 l_0^2} \sum_{\lambda, \zeta = \pm} \sum_{n=1}^{\infty} f(\varepsilon_{n,\zeta}^\lambda) \left\{ 1 - f(\varepsilon_{n,\zeta}^\lambda) \right\} \times \int_0^\infty u \left| F_{n\lambda}^\zeta(u) \right|^2 du. \quad (14)$$

Using the orthogonality of the Laguerre polynomials i. e. $\int_0^\infty e^{-x} L_m(x) L_n(x) dx = \delta_{nm}$ and the recurrence relation $(n+1)L_{n+1}(x) = (2n+1-x)L_n(x) - nL_{n-1}(x)$, one can do the integration in Eq. (14). Finally, we have

$$\sigma_{yy} = g_s \frac{e^2 \beta n_{\text{im}} U_0^2}{h 4\pi \Gamma_0 l_0^2} \sum_{\lambda, \zeta} \sum_{n=1}^{\infty} f(\varepsilon_{n,\zeta}^\lambda) \left\{ 1 - f(\varepsilon_{n,\zeta}^\lambda) \right\} I_{n\lambda}^\zeta \quad (15)$$

where

$$I_n^\zeta = (2n-1)|A_n^\zeta|^2 + (2n+1) + (2n+3)|B_n^\zeta|^2 - 2nA_n^\zeta - 2(n+1)B_n^\zeta$$

with $A_n^\zeta = n(1 - \chi_\zeta)/(n + \chi_\zeta)$ and $B_n^\zeta = (n+1)\chi_\zeta/(n + \chi_\zeta)$.

Additionally, the zeroth Landau level would contribute the following amount to the conductivity

$$\sigma_{yy}^0 = g_s \frac{e^2 \beta n_{\text{im}} U_0^2}{h 2\pi \Gamma_0 l_0^2} \sum_{\lambda, \zeta} f(\varepsilon_{0,\zeta}^\lambda) \left\{ 1 - f(\varepsilon_{0,\zeta}^\lambda) \right\}. \quad (16)$$

B. Hall Conductivity

Another important quantity of the linear response theory is the Hall conductivity. Its general expression is given by²⁶⁻²⁹

$$\sigma_{yx} = \frac{i\hbar e^2}{S} \sum_{\xi, \xi'} \frac{(f_\xi - f_{\xi'}) \langle \xi | v_x | \xi' \rangle \langle \xi' | v_y | \xi \rangle}{(\varepsilon_\xi - \varepsilon_{\xi'}) (\varepsilon_\xi - \varepsilon_{\xi'} + i\Gamma_0)}. \quad (17)$$

Here, $f_\xi \equiv f(\varepsilon_\xi)$. The expressions for matrix elements of velocity operators i.e. $\langle \xi | v_i | \xi' \rangle$ with $i = x, y$ are given in the Appendix B. As those contain $\delta_{k'_x, k_x}$, the summation in Eq. (17) can be simplified as

$$\sum_{\xi, \xi'} \longrightarrow g_s \frac{S}{2\pi l_0^2} \sum_{n, n', \lambda, \lambda'}.$$

Finite broadening of the Landau levels has been considered for the collisional conductivity. In the case of the Hall conductivity, only the transition between different Landau levels is important. For sharp levels, the results would be more appropriate. Hence, we take $\Gamma_0 = 0$ for simplicity. Now, Eq. (17) becomes

$$\sigma_{yx} = g_s \frac{i\hbar e^2}{2\pi l_0^2} \sum_{n, n', \lambda, \lambda'} \frac{(f_n^\lambda - f_{n'}^{\lambda'}) Q_{nn'}^{\lambda\lambda'}}{(\varepsilon_n^\lambda - \varepsilon_{n'}^{\lambda'})^2}, \quad (18)$$

where $Q_{nn'}^{\lambda\lambda'} = \langle \Psi_n^\lambda | v_x | \Psi_{n'}^{\lambda'} \rangle \langle \Psi_{n'}^{\lambda'} | v_y | \Psi_n^\lambda \rangle$. Note that, the valley index ζ is omitted from Eq. (18). We will calculate σ_{yx} individually for different valleys and restore the index ζ later.

It is worthy to mention that two different kind of transitions are possible to occur. One is transitions between various states within the conic band. The other type is the transition from the flat band to the conic band and vice versa. Let us discuss both the contributions one by one.

1. Transitions within the Conic Band

Since the wave function corresponding to $n = 0$ and $n > 0$ Landau levels are different, we expand the summation in Eq. (18) explicitly as

$$\sigma_{yx}^C = D \left[\sum_{n, \lambda, \lambda'} \frac{f_n^\lambda - f_0^{\lambda'}}{(\varepsilon_n^\lambda - \varepsilon_0^{\lambda'})^2} Q_{n0}^{\lambda, \lambda'} + \sum_{n', \lambda, \lambda'} \frac{f_0^\lambda - f_{n'}^{\lambda'}}{(\varepsilon_0^\lambda - \varepsilon_{n'}^{\lambda'})^2} Q_{0n'}^{\lambda, \lambda'} + \sum_{n, n', \lambda, \lambda'} \frac{(f_n^\lambda - f_{n'}^{\lambda'}) Q_{nn'}^{\lambda\lambda'}}{(\varepsilon_n^\lambda - \varepsilon_{n'}^{\lambda'})^2} \right], \quad (19)$$

where the symbol C is used to denote the conic band and $D = ig_s \hbar e^2 / (2\pi l_0^2)$.

The explicit expressions of $Q_{n0}^{\lambda\lambda'}$, $Q_{0n'}^{\lambda\lambda'}$, and $Q_{nn'}^{\lambda\lambda'}$ are given by

$$Q_{n0}^{\lambda\lambda'} = i \frac{v_F^2}{4} \left(\lambda' \frac{\sqrt{n}(1 - \chi_\zeta)}{\sqrt{n} + \chi_\zeta} + \lambda \sqrt{\chi_\zeta} \right)^2 \delta_{n1}, \quad (20)$$

$$Q_{0n'}^{\lambda\lambda'} = -i \frac{v_F^2}{4} \left(\lambda \frac{\sqrt{n'}(1 - \chi_\zeta)}{\sqrt{n'} + \chi_\zeta} + \lambda' \sqrt{\chi_\zeta} \right)^2 \delta_{n'1}, \quad (21)$$

and

$$Q_{nn'}^{\lambda\lambda'} = i \frac{v_F^2}{4} \left(|M_{nn'}^{\lambda\lambda'}|^2 \delta_{n'n-1} - |N_{nn'}^{\lambda\lambda'}|^2 \delta_{n'n+1} \right). \quad (22)$$

Here, the explicit forms of $|M_{nn'}^{\lambda\lambda'}|^2$ and $|N_{nn'}^{\lambda\lambda'}|^2$ are given in the Appendix B.

To evaluate σ_{yx}^C , we note that four different types of the set (λ, λ') are possible to include all the transitions. They are $(+, +)$, $(-, -)$, $(+, -)$, and $(-, +)$. Considering

all the contributions, we, finally, arrive at the following expression for the Hall conductivity

$$\sigma_{yx}^C = \frac{g_s e^2}{2h} \sum_{\zeta} \sum_{n=0}^{\infty} (n+1) P_{n,n+1}^{\zeta} \left[f_n^{+, \zeta} + f_n^{-, \zeta} - f_{n+1}^{+, \zeta} - f_{n+1}^{-, \zeta} \right], \quad (23)$$

where

$$P_{n,n+1}^{\zeta} = \left[1 + \left(\frac{\delta_n^{\zeta}}{\delta_{n+1}^{\zeta}} \right)^2 \right] (1 - \chi_{\zeta})^2 + \left[1 + \left(\frac{\delta_{n+1}^{\zeta}}{\delta_n^{\zeta}} \right)^2 \right] \chi_{\zeta}^2 + 4\chi_{\zeta}(1 - \chi_{\zeta}), \quad (24)$$

with $\delta_n^{\zeta} = \sqrt{n + \chi_{\zeta}}$.

2. Transition between Conic band and Flat band

The electronic transitions from the flat band to the conic band and vice-versa produce a finite contribution to the Hall conductivity. Particularly, it is crucial for low-density where small number of Landau levels contribute to the summation. The resulting contribution can be written as

$$\sigma_{yx}^{CF} = 2D \sum_{\lambda'} \left[\frac{f_0^{\lambda'} - f_0^F}{(\varepsilon_0^{\lambda'} - \varepsilon_0^F)^2} Q_{00\lambda'}^{FC} + \sum_{n=1}^{\infty} \frac{f_0^{\lambda'} - f_n^F}{(\varepsilon_0^{\lambda'} - \varepsilon_n^F)^2} Q_{0n\lambda'}^{FC} \right] + \sum_{n'=1}^{\infty} \frac{f_{n'}^{\lambda'} - f_0^F}{(\varepsilon_{n'}^{\lambda'} - \varepsilon_0^F)^2} Q_{n'0\lambda'}^{FC} + \sum_{n \neq n'}^{\infty} \frac{f_{n'}^{\lambda'} - f_n^F}{(\varepsilon_{n'}^{\lambda'} - \varepsilon_n^F)^2} Q_{n'n\lambda'}^{FC}, \quad (25)$$

where $Q_{n'n\lambda'}^{CF} = \langle \Psi_{n'}^{\lambda'} | v_x | \Psi_n^F \rangle \langle \Psi_n^F | v_y | \Psi_{n'}^{\lambda'} \rangle$. The factor '2' in Eq. (25) arises due to the fact that transition is possible from the conic band to the flat band and vice-versa.

By calculating all $Q_{n'n\lambda'}^{CF}$ explicitly for the valley ζ , Eq. (25) can be reduced further into the following simplified form

$$\sigma_{yx\zeta}^{CF} = \frac{g_s e^2}{2h} \left[\left(2\zeta \frac{1 - \chi_{\zeta}}{1 + \chi_{\zeta}} - 1 \right) (f_0^{+\zeta} + f_0^{-\zeta} - 2f_0^F) + \chi_{\zeta}(1 - \chi_{\zeta}) \sum_{n=1}^{\infty} \frac{(n+2)G_n^{\zeta} - nG_{n+1}^{\zeta}}{(n + \chi_{\zeta})(n + 1 + \chi_{\zeta})} \right], \quad (26)$$

where $G_n^{\zeta} = f_n^{+\zeta} + f_n^{-\zeta} - 2f_n^F$. In deriving Eq. (26), we have also used the fact $f_n^F = f_{n+1}^F$ since $\varepsilon_n^F = 0 \forall n$. By summing up the contributions corresponding to the different valleys we would obtain the net Hall conductivity due to the flat-conic band transitions and this amount adds up to Eq. (23) in order to obtain the total Hall conductivity.

IV. RESULTS AND DISCUSSIONS

Here, we discuss various features of the collisional and Hall conductivities obtained through the numerical evaluation of Eqs. (15), (16), (23), and (26). To do this we

use the following parameters: $\epsilon_r = 2.5$, $k_s = 10^8 \text{ m}^{-1}$, and $n_{\text{im}} = 1.5 \times 10^{13} \text{ m}^{-2}$. We also consider $\Gamma_0 = 0.07\gamma_B$ that means $\Gamma_0 \propto \sqrt{B}$. The existence of this behavior of Γ_0 has been confirmed in Refs.[3,30].

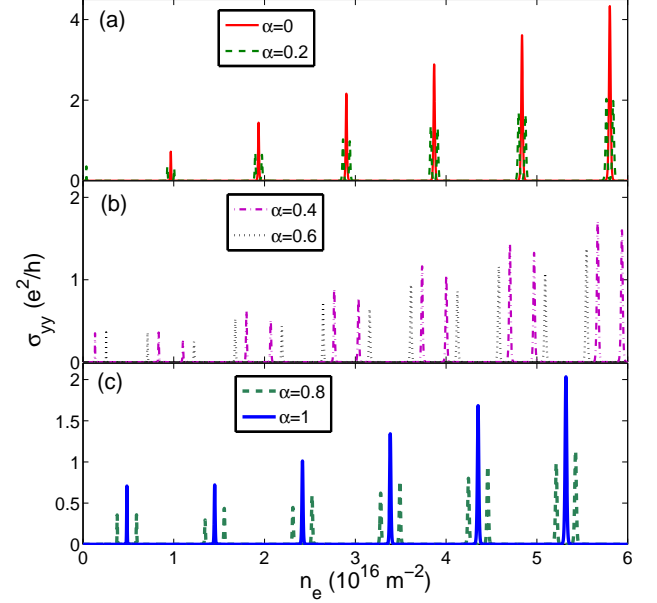


FIG. 2: (Color online) Plots of the collisional conductivity with the electron density for various values of α . The magnetic field is fixed to a value $B = 10 \text{ T}$.

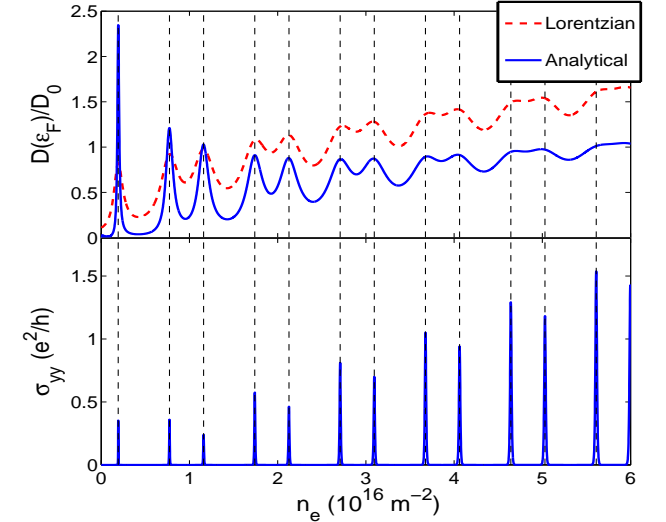


FIG. 3: (Color online) Plots of DOS and collisional conductivity with the electron density for $\alpha = 0.5$. The magnetic field is fixed to a value $B = 10 \text{ T}$. Here, $D_0 = 1/(l_0^2 \gamma_B)$. In the upper panel, the actual value of the solid (blue) line is reduced by a factor π for a better visualization.

The variation of the collisional conductivity (σ_{yy}) with

electron density (n_e) is depicted in Fig. 2 for a constant magnetic field, namely, $B = 10$ T and different values of α , namely, $\alpha = 0, 0.2, 0.4, 0.6, 0.8, 1$. When $\alpha = 0$ (resembles the case of graphene), σ_{yy} displays oscillatory behavior consisting of a number of peaks. This situation changes dramatically as we switch on the parameter α . For a finite α , each conductivity peak splits into two peaks which are unequal in magnitude. The splitting of the peaks can be attributed to the phase difference between the contributions arising from different valleys. Additionally, a single peak appears at very lower density which was absent in the case of graphene. This appearance is a direct consequence of the fact that unlike graphene the $n = 0$ Landau level is not shared by the conduction and valence bands. They are distinct in energy separated by a gap of $2\sqrt{\chi\zeta}$ for valley ζ . In other words, the so called “quantum anomaly” of $n = 0$ level for graphene is absent in the α - T_3 model. With the increase of α , the gap between two split peaks increases. More specifically, two peaks move in opposite directions. Furthermore, the position of the single peak moves towards higher density. Eventually, it merges with the left split-peak of the 2nd peak when α reaches 1. Similarly, as α approaches 1 the right split-peak of the 2nd peak merges with the left split-peak of the 3rd peak and so on. As a result, for $\alpha = 1$ we obtain a new set of conductivity peaks whose positions are completely different than graphene.

The origin of splitting of the conductivity peaks will become more transparent if we explore the behavior of the density of states (DOS) at the Fermi energy. The motivation behind this is the fact that any transport related quantity is proportional to the DOS at the Fermi energy. Generally, the DOS of the Landau levels is given by $D(\varepsilon) = \sum \delta(\varepsilon - \varepsilon_{n,\zeta}^\lambda)$. Since the levels are broadened by impurities, we can replace the δ -function by a Lorentzian distribution as discussed in section III(A). Hence, the DOS has to be calculated numerically. However, it is possible to obtain the following approximate analytical expression of the DOS (the derivation is given in Appendix C),

$$D(\varepsilon_F) = \frac{2\varepsilon_F}{\pi l_0^2 \gamma_B^2} \sum_{\zeta} \left\{ 1 + 2 \sum_{k=1}^{\infty} \exp \left[-2k \left(\frac{2\pi \Gamma_0 \varepsilon_F}{\gamma_B^2} \right)^2 \right] \times \cos \left[2k\pi \left(\frac{\varepsilon_F^2}{\gamma_B^2} - \chi_{\zeta} \right) \right] \right\}. \quad (27)$$

The DOS at the Fermi energy, calculated numerically and from Eq. (27), are depicted in Fig. 3 for a given $\alpha = 0.5$. From Fig. 3, we may conclude that $D(\varepsilon_F)$ displays similar features as σ_{yy} i.e. splitting of peaks and the position of peaks in $D(\varepsilon_F)$ and σ_{yy} are the same. By considering the most dominant first harmonics ($k = 1$ term) only in Eq. (27), we may write $D_{\zeta}(\varepsilon_F) \sim \cos(\pi^2 l_0^2 n_e - 2\pi \chi_{\zeta})$. This clearly indicates that two valleys contribute different amounts to the DOS which differ by a phase $2\pi(\chi_- - \chi_+) = 2\pi(1 - \alpha^2)/(1 + \alpha^2)$. This phase differ-

ence lies entirely behind the splitting of the conductivity peaks.

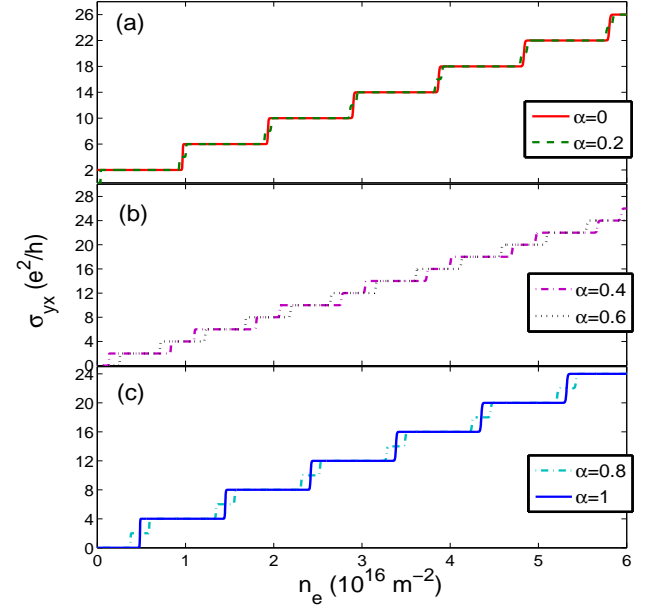


FIG. 4: (Color online) Plots of the Hall conductivity versus electron density for different values of α at fixed $B = 10$ T.

In Fig. 4, we have shown the behavior of the Hall conductivity as a function of the electron density. We fix $B = 10$ T and tune α from 0 to 1. For $\alpha = 0$ (graphene), σ_{yx} contains a series of Hall plateaus of values 2, 6, 10, ... in units of e^2/h . This type of quantization occurs due to the “quantum anomaly” of the lowest Landau level⁴. A finite α introduces a new series of plateaus situated at the midway between every two plateaus. Additionally, a plateau at which $\sigma_{yx} = 0$ appears due to the fact the lowest Landau-level has non-zero energy and its degeneracy is lifted by a factor ‘2’ in presence of a finite α . Thus at finite α , one obtains the following Hall quantization $\sigma_{yx} = 2ne^2/h$ with $n = 0, 1, 2, \dots$. The width of each new plateau increases and that of each old plateau shrinks with the evolution of α from 0 to 1. Finally, a new series of plateaus of values 0, 4, 8, ... in units of e^2/h is obtained for $\alpha = 1$. Our results are similar to the findings of Ref.[21] in which DC Hall conductivity was indirectly derived from magnetization using the Streda formula³¹. Here, we obtain Hall quantization directly via the implementation of the Kubo formalism. In Ref.[21], the contribution of flat band was completely ignored due to its zero energy. However, in our treatment the transitions between the flat and conic band plays a crucial role, particularly at lower density in order to get accurate quantization of the Hall conductivity.

The behavior of the resistivity with magnetic field for $\alpha = 0.5$ is shown in Fig. 5. For every jump in the Hall resistivity from a plateau to the next one, a peak appears in the longitudinal resistivity.

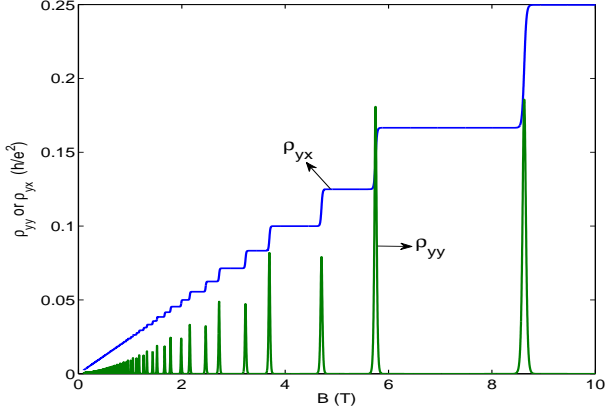


FIG. 5: (Color online) Plots of ρ_{yy} and ρ_{yx} with magnetic field for $\alpha = 0.5$. For better visualization, the actual data for ρ_{yy} are enhanced by a factor 20.

V. SUMMARY

In this work, we have explored the magneto-transport properties of the α - T_3 model by evaluating collisional and the Hall conductivities using the standard Kubo formula. At strong magnetic field a number of peaks is appearing in the collisional conductivity. The conductivity peaks split into two as a consequence of lifting of the valley degeneracy in presence of finite α except at $\alpha = 1$. The origin of this splitting has also been explained through the behavior of density of states, calculated numerically and analytically. A new series of conductivity peaks is obtained for $\alpha = 1$ which is different than $\alpha = 0$ case. Like graphene, the Hall conductivity behaves like $\sigma_{yx} = 2(2n+1)e^2/h$ with $n = 0, 1, 2, \dots$ for $\alpha = 0$. At finite α , additional plateaus appear exactly at the mid way between every two Hall plateaus. The width of each new (old) plateau increases (decreases) as α increases from 0 to 1. Thus, one obtains the following Hall quantization $\sigma_{yx} = 4ne^2/h$ with $n = 0, 1, 2, \dots$ for $\alpha = 1$.

Acknowledgement

We would like to thank SK Firoz Islam and Alestin Mawrie for useful discussions.

Appendix A

1. Wave functions in K' -valley

For the conic band, the eigen functions corresponding to $n > 0$ and $n = 0$ are given by

$$\Psi_{n,k_x}^{\lambda,K'}(\mathbf{r}) = \frac{1}{\sqrt{2}} \begin{pmatrix} \frac{\sqrt{(n+1)\chi_-}}{\sqrt{n+\chi_-}} \Phi_{n+1}(y) \\ -\lambda \Phi_n(y) \\ \frac{\sqrt{n(1-\chi_-)}}{\sqrt{n+\chi_-}} \Phi_{n-1}(y) \end{pmatrix} \frac{e^{ik_x x}}{\sqrt{2\pi}}. \quad (\text{A1})$$

and

$$\Psi_{0,k_x}^{\lambda,K'}(\mathbf{r}) = \frac{1}{\sqrt{2}} \begin{pmatrix} \Phi_1(y) \\ -\lambda \Phi_0(y) \\ 0 \end{pmatrix} \frac{e^{ik_x x}}{\sqrt{2\pi}} \quad (\text{A2})$$

The flat-band wave functions are given by

$$\Psi_{n,k_x}^{F,K'}(\mathbf{r}) = \begin{pmatrix} -\frac{\sqrt{n(1-\chi_-)}}{\sqrt{n+\chi_-}} \Phi_{n+1}(y) \\ 0 \\ \frac{\sqrt{(n+1)\chi_-}}{\sqrt{n+\chi_-}} \Phi_{n-1}(y) \end{pmatrix} \frac{e^{ik_x x}}{\sqrt{2\pi}}, \quad (\text{A3})$$

for $n > 0$ and

$$\Psi_{0,k_x}^{F,K'}(\mathbf{r}) = \begin{pmatrix} \Phi_0(y) \\ 0 \\ 0 \end{pmatrix} \frac{e^{ik_x x}}{\sqrt{2\pi}}, \quad (\text{A4})$$

for $n = 0$.

Appendix B

1. Matrix elements of the velocity operators

The matrix elements of the velocity components for a given valley ζ can be obtained as

$$\langle \Psi_{nk_x}^{\lambda\zeta} | v_x | \Psi_{n'k'_x}^{\lambda'\zeta} \rangle = \frac{v_F}{2} b \left(M_{nn'}^{\lambda\lambda'} \delta_{n',n-1} + N_{nn'}^{\lambda\lambda'} \delta_{n',n+1} \right) \quad (\text{B1})$$

and

$$\langle \Psi_{n'k'_x}^{\lambda'\zeta} | v_y | \Psi_{nk_x}^{\lambda\zeta} \rangle = \frac{iv_F}{2} b \left(M_{nn'}^{\lambda\lambda'} \delta_{n',n-1} - N_{nn'}^{\lambda\lambda'} \delta_{n',n+1} \right) \quad (\text{B2})$$

where

$$M_{nn'}^{\lambda\lambda'} = \lambda \frac{\sqrt{n'+1}\chi_\zeta}{\sqrt{n'+\chi_\zeta}} + \lambda' \frac{\sqrt{n}(1-\chi_\zeta)}{\sqrt{n+\chi_\zeta}}, \quad (\text{B3})$$

$$N_{nn'}^{\lambda\lambda'} = \lambda \frac{\sqrt{n'}(1-\chi_\zeta)}{\sqrt{n'+\chi_\zeta}} + \lambda' \frac{\sqrt{n+1}\chi_\zeta}{\sqrt{n+\chi_\zeta}} \quad (\text{B4})$$

and $b = \delta_{k_x, k'_x}$.

For $0 \rightarrow n$ scattering, we have the following matrix elements of v_x and v_y

$$\langle \Psi_{0k'_x}^\zeta | v_x | \Psi_{nk_x}^\zeta \rangle = \frac{v_F}{2} b \left[\lambda' \frac{\sqrt{n}(1 - \chi_\zeta)}{\sqrt{n' + \chi_\zeta}} + \lambda \sqrt{\chi_\zeta} \right] \delta_{n,1}$$

and

$$\langle \Psi_{nk_x}^\zeta | v_y | \Psi_{0k'_x}^\zeta \rangle = \frac{-iv_F}{2} b \left[\lambda' \frac{\sqrt{n}(1 - \chi_\zeta)}{\sqrt{n' + \chi_\zeta}} + \lambda \sqrt{\chi_\zeta} \right] \delta_{n,1}.$$

Appendix C

1. Calculation of density of states

Here, we provide an explicit calculation of the density of states (DOS) of the Landau levels which are broadened by impurities. To calculate DOS, we may start from the following expression of the associated self-energy^{32,33},

$$\Sigma^-(\varepsilon) = \Gamma_0^2 \sum_{n,\zeta} \frac{1}{\varepsilon - \varepsilon_{n,\zeta}^\lambda - \Sigma^-(\varepsilon)}. \quad (\text{C1})$$

The imaginary part of $\Sigma^-(\varepsilon)$ is directly related to DOS via

$$D(\varepsilon) = \text{Im} \left[\frac{\Sigma^-(\varepsilon)}{\pi^2 l_0^2 \Gamma_0^2} \right]. \quad (\text{C2})$$

The summation over n in Eq. (C1) can be evaluated with the help of residue theorem i. e. $\sum_n g(n) =$

$-\{ \text{Sum of residues of } \pi \cot(\pi z) g(z) \text{ at all poles of } g(z) \}$. Inserting $\varepsilon_{n,\zeta}^\lambda$ in Eq. (C1) we can identify $g(n)$ as $g(n) = a/(b - c\sqrt{n + \chi_\zeta})$, where $a = \Gamma_0^2$, $b = \varepsilon - \Sigma^-(\varepsilon)$, and $c = \lambda\gamma_B$. Now, the function $g(z)$ has a pole at $z_0 = b^2/c^2 - \chi_\zeta$. The residue of $\pi \cot(\pi z) g(z)$ is $-(2ab/c^2)\pi \cot[\pi(b^2/c^2 - \chi_\zeta)]$. Considering the terms which are only linear in $\Sigma^-(\varepsilon)$, the self-energy can be approximated to the following form

$$\Sigma^-(\varepsilon) \simeq \frac{2\pi\Gamma_0^2\varepsilon}{\gamma_B^2} \cot \left[\pi \left\{ \frac{(\varepsilon^2 - 2\varepsilon\Sigma^-(\varepsilon))}{\gamma_B^2} \right\} - \chi_\zeta \right]. \quad (\text{C3})$$

Separating $\Sigma^-(\varepsilon)$ into real and imaginary parts i. e. $\Sigma^-(\varepsilon) = \Delta(\varepsilon) + i\Gamma(\varepsilon)/2$, Eq. (C3) can be rewritten as $\Sigma^-(\varepsilon) \simeq (2\pi\Gamma_0^2\varepsilon/\gamma_B^2) \cot(u - iv)$, where $u = \pi[(\varepsilon^2 - 2\varepsilon\Delta(\varepsilon))/\gamma_B^2 - \chi_\zeta]$ and $v = \pi\varepsilon\Gamma(\varepsilon)/\gamma_B^2$. Now, it is straightforward to obtain the imaginary part of the self-energy as

$$\begin{aligned} \frac{\Gamma(\varepsilon)}{2} &= \frac{2\pi\Gamma_0^2\varepsilon}{\gamma_B^2} \frac{\sinh(2v)}{\cosh(2v) - \cos(2u)} \\ &= \frac{2\pi\Gamma_0^2\varepsilon}{\gamma_B^2} \left[1 + 2 \sum_{k=1}^{\infty} e^{-2kv} \cos(2ku) \right]. \end{aligned} \quad (\text{C4})$$

In the limit $\pi\varepsilon\Gamma(\varepsilon)/\gamma_B^2 \ll 1$, $\Gamma(\varepsilon)$ can be obtained iteratively from Eq. (C4). After first iteration, we get $\Gamma(\varepsilon) = 4\pi\Gamma_0^2\varepsilon/\gamma_B^2$. Consequently, the DOS is obtained in the following form

$$D(\varepsilon) = \frac{2\varepsilon}{\pi l_0^2 \gamma_B^2} \sum_{\zeta} \left\{ 1 + 2 \sum_{k=1}^{\infty} \exp \left[-2k \left(\frac{2\pi\Gamma_0^2\varepsilon}{\gamma_B^2} \right)^2 \right] \cos \left[2k\pi \left(\frac{\varepsilon^2}{\gamma_B^2} - \chi_\zeta \right) \right] \right\}. \quad (\text{C5})$$

* Electronic address: tbtutulm53@gmail.com

† Electronic address: tkghosh@iitk.ac.in

¹ K. S. Novoselov, A. K. Geim, S. V. Morozov, D. Jiang, Y. Zhang, S. V. Dubonos, I. V. Grigorieva, and A. A. Firsov, *Science* **306**, 666 (2004).

² K. S. Novoselov, A. K. Geim, S. V. Morozov, D. Jiang, M. I. Katsnelson, I. V. Grigorieva, S. V. Dubonos, A. A. Firsov, *Nature* **438**, 197 (2005).

³ Y. Zheng and T. Ando, *Phys. Rev. B* **65**, 245420 (2002).

⁴ V. P. Gusynin and S. G. Sharapov, *Phys. Rev. Lett.* **95**, 146801 (2005).

⁵ Y. Zhang, Y.-W. Tan, H. L. Stormer, and P. Kim, *Nature (London)* **438**, 201 (2005).

⁶ K. S. Novoselov, Z. Jiang, Y. Zhang, S. V. Morozov, H. L.

Stormer, U. Zeitler, J. C. Maan, G. S. Boebinger, P. Kim, and A. K. Geim, *Science* **315**, 1379 (2007).

⁷ B. Sutherland, *Phys. Rev. B* **34**, 5208 (1986).

⁸ J. Vidal, R. Mosseri, and B. Doucot, *Phys. Rev. Lett.* **81**, 5888 (1998).

⁹ S. E. Korshunov, *Phys. Rev. B* **63**, 134503 (2001).

¹⁰ M. Rizzi, V. Cataudella, and R. Fazio, *Phys. Rev. B* **73**, 144511 (2006).

¹¹ D. Bercioux, M. Governale, V. Cataudella, and V. M. Ramaglia, *Phys. Rev. Lett.* **93**, 056802 (2004); *Phys. Rev. B* **72**, 075305 (2005).

¹² D. F. Urban, D. Bercioux, M. Wimmer, and W. Häusler, *Phys. Rev. B* **84**, 115136 (2011).

¹³ J. D. Malcolm and E. J. Nicol, *Phys. Rev. B* **93**, 165433

- (2016).
- ¹⁴ D. Bercioux, D. F. Urban, H. Grabert, and W. Häusler, *Phys. Rev. A* **80**, 063603 (2009).
 - ¹⁵ F. Wang and Y. Ran, *Phys. Rev. B* **84**, 241103 (2011).
 - ¹⁶ B. Dora, J. Kailasvuori, and R. Moessner, *Phys. Rev. B* **84**, 195422 (2011).
 - ¹⁷ Z. Lan, N. Goldman, A. Bermudez, W. Lu, and P. Öhberg, *Phys. Rev. B* **84**, 165115 (2011).
 - ¹⁸ J. D. Malcolm and E. J. Nicol, *Phys. Rev. B* **90**, 035405 (2014).
 - ¹⁹ A. Raoux, M. Morigi, J.-N. Fuchs, F. Piechon, and G. Montambaux, *Phys. Rev. Lett.* **112**, 026402 (2014).
 - ²⁰ J. D. Malcolm and E. J. Nicol, *Phys. Rev. B* **92**, 035118 (2015).
 - ²¹ E. Illes, J. P. Carbotte, and E. J. Nicol, *Phys. Rev. B* **92**, 245410 (2015).
 - ²² A. D. Kovacs, G. David, B. Dora, and J. Cserti, *arXiv:1605.09588*.
 - ²³ E. Illes, and E. J. Nicol, *arXiv:1606.00823*.
 - ²⁴ G. M. Eliashberg, *Sov. Phys.-JETP* **14**, 886 (1962).
 - ²⁵ M. Charbonneau, K. M. Van Vliet, and P. Vasilopoulos, *J. Math. Phys.* **23**, 318 (1982).
 - ²⁶ P. Vasilopoulos, *Phys. Rev. B* **32**, 771 (1985).
 - ²⁷ F. M. Peeters and P. Vasilopoulos, *Phys. Rev. B* **46**, 4667 (1992).
 - ²⁸ X. F. Wang and P. Vasilopoulos, *Phys. Rev. B* **67**, 085313 (2003).
 - ²⁹ P. M. Krstajic and P. Vasilopoulos, *Phys. Rev. B* **83**, 075427 (2011).
 - ³⁰ M. E. Raikh and T. V. Shahbazyan, *Phys. Rev. B* **47**, 1522 (1993).
 - ³¹ P. Streda, *J. Phys. C* **15**, L717 (1982).
 - ³² T. Ando, A. B. Fowler, and F. Stern, *Rev. Mod. Phys.* **54**, 437 (1982).
 - ³³ C. Zhang and R. R. Gerhardts, *Phys. Rev. B* **41**, 12850 (1990).